U-Th dating of striated fault planes

Perach Nuriel[1]*, Gideon Rosenbaum[1], Jian-Xin Zhao[2], Yuexing Feng[2], Suzanne D. Golding[1], Benoît Villemant[3], and Ram Weinberger[4]

[1]School of Earth Sciences, The University of Queensland, Brisbane, QLD 4072, Australia
[2]Radiogenic Isotope Laboratory, Centre for Microscopy and Microanalysis (CMM), The University of Queensland, Brisbane St Lucia, QLD 4072, Australia
[3]Laboratoire de Pétrologie, Géochimie, Volcanologie, UPMC University Pierre et Marie Curie - Paris 6, UMR 7193, ISTeP, 4 place Jussieu, F-75005 Paris, France
[4]Geological Survey of Israel, 30 Malkhe Israel Street, Jerusalem 95501, Israel

ABSTRACT

Direct dating of brittle fault activity is of fundamental importance to tectonic reconstructions and paleoseismic studies. One way to address this issue is by constraining the timing of fault striations, but this requires a better understanding of the striation formation mechanism and associated mineralization. We present results from a microstructural, geochemical, and geochronological study of calcite precipitates associated with striated fault planes from the Dead Sea fault zone in northern Israel. We recognize four types of coexisting calcite precipitates, including calcite cement in dilation breccia, calcite in striated groove morphology, calcite gouge associated with hydraulic fracturing and pressure solution, and calcite coating of the fault surface. Carbon-oxygen isotopes, $^{87}Sr/^{86}Sr$ ratios, and rare earth element and yttrium (REY) patterns indicate various precipitation mechanisms associated with formation of syntectonic (calcite cement and striations), coseismic (calcite gouge), and interseismic (calcite coating) precipitates in the fault zone. Using U-Th dating of samples from three adjacent fault planes, we delineate four well-defined deformation ages in the period from 220 to 60 ka. We conclude that these ages constrain the timing of activity along the Dead Sea fault zone in northern Israel, and argue that a similar methodological approach could potentially shed light on the timing of deformation in other brittle fault zones.

INTRODUCTION

The formation of fault striations is considered to result from frictional forces applied to the fault surface, leading to the scratching of grooves parallel to the slip direction (e.g., Petit, 1987; Doblas, 1998). In many cases, the striated surface incorporates newly mineralized material that precipitated either during fault movement or after deformation (Gamond, 1983; Gratier and Gamond, 1990). Dating such minerals, as demonstrated by Eyal et al. (1992) on the uranium-bearing mineral carnotite, can potentially constrain the timing of fault activity, thus providing a reliable chronological tool for paleoseismic and neotectonic research.

Recent advances in U-series geochronology and instrumentation offer a challenging opportunity for direct dating of minerals that are less uranium-rich and more abundant, such as calcite. In addition, current analytical capabilities enable U-Th dating of very small amounts of material, meaning that calcite can be extracted selectively from fault-related microstructures. This approach requires a better understanding of the precipitation mechanisms associated with the formation of fault striations, and the temporal relationships between faulting, dissolution, fluid mobilization, and calcite precipitation.

Temporal relations between calcite precipitation and faulting include (1) coseismic crystallization within hydraulic fractures (Boullier et al., 2004; Uysal et al., 2007), (2) syntectonic crystallization within fault-related dilation structures (Boles and Grivetti, 2000; Verhaert et al., 2003, 2004; Watanabe et al., 2008; Nuriel et al., 2011), (3) postcrystallization shearing involving pressure solution and recrystallization (Laurent, 1987; Eyal et al., 1992), and (4) interseismic precipitation within dilation structures, such as coating of striated fault surfaces (Flotté et al., 2001) and open-mode fractures (Verhaert et al., 2004; Nuriel et al., 2011). While coseismic and interseismic precipitates are likely to coexist in fault zones, the various types of calcite precipitates have seldom been studied within a single fault. Taking such an approach can provide insights into the spatial and temporal variations of calcite precipitation during the seismic cycle.

This paper focuses on striated fault planes within the seismically active Dead Sea fault zone, which is a left-lateral transform fault that accommodates the relative motion between the Arabian plate and Sinai subplate (e.g., Garfunkel, 1981) (Fig. 1A). We present evidence for the formation mechanisms of fault surfaces, striations, hydraulic fractures, and dilation breccias, and constrain the timing of formation of the different types of calcite precipitates. Our results demonstrate that a prolonged history of seismic and interseismic activity is recorded in the microstructures, geochemistry, and U-Th ages.

METHODOLOGY

Calcite microsamples were extracted from oriented hand specimens using hand drills or hand pliers. Analyses were carried out at the Stable Isotope Geochemistry Laboratory and the Radiogenic Isotope Laboratory, at the University of Queensland (Australia). Stable isotope measurements were obtained using an Isoprime Dual Inlet stable isotope ratio mass spectrometer (SIRMS). $^{87}Sr/^{86}Sr$ isotope ratios were measured in a three-cycle dynamic mode on a VG Sector-54 thermal ionization mass spectrometer (TIMS). Trace element measurements were performed on a Thermo X-series inductively coupled plasma–mass spectrometer (ICP-MS). U-series dating was carried out by a Nu

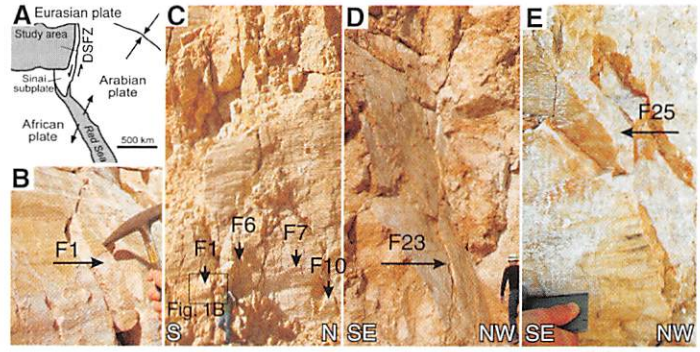

Figure 1. A: Location map showing regional setting of the Dead Sea fault zone (DSFZ), Israel. B–E: Studied fault planes and approximate locations of samples F1, F6, F7, F10, F23, and F25.

*E-mail: pnuriel@gmail.com.

Plasma multicollector ICP-MS under conditions described by Zhou et al. (2011). Detailed sampling and analytical procedures are described in the GSA Data Repository[1].

RESULTS

Structural Observations and Field Sampling

Three fault planes were studied along the Dead Sea fault zone in northern Israel (Fig. 1). They are a part of a major set of subsidiary northwest- to northeast-striking left-lateral faults in the Kefar Giladi quarry, described in detail elsewhere (Weinberger et al., 2009; Nuriel et al., 2012). Four different localities along one vertical north-south fault plane were sampled (F1, F6, F7 and F10; Fig. 1C), all of which show prominent subhorizontal striations (Fig. 1B). The two other planes are subvertical northwest-southeast–striking faults, located ~100 m apart, and showing prominent subhorizontal striations (F23 and F25; Figs. 1D and 1E). Polished hand-sized slabs, which were cut perpendicular to the fault planes, revealed that the mesoscale striated fault structure consists of host-rock breccias and calcite precipitates (up to 50% in volume). From each fault plane, samples were divided into fragments, from which the different types of calcite precipitates were separated (see Fig. DR1 in the Data Repository).

Microstructures

Based on optical microscopy, cathodoluminescence (CL), and scanning electron microscope (SEM) examination, four types of fault-related calcite precipitates were identified (Fig. 2):

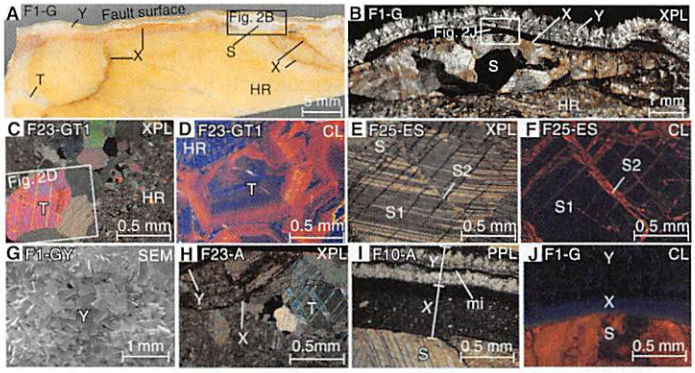

Figure 2. Microstructure of calcite precipitates within striated fault planes. Labels indicate sample name and the type of image (XPL—cross-polarized light; PPL—plane-polarized light; CL—cathodoluminescence light; SEM—scanning electron microscope). HR—host rock. A: Polished slab of a hand specimen taken perpendicular to fault plane and grooves showing the coexisting calcite precipitates (cement [T], striations [S], gouge [X], and coating [Y]). B: Close-up of calcite striations (location is shown in A). C: Calcite cement with twinned grains. D: Close-up of C, showing zoning under CL light. E: Straight and thin twinned calcite striations with sutured boundaries. F: Same as E, but showing bright CL colors (S2) as opposed to the dark CL colors of the host grain (S1). G: Top view (parallel to striations) of a calcite coating layer showing perfect rhombic shape of calcite crystals. H: Occurrence of calcite gouge in a complex veinlet network within trans-granular fractures (postdates calcite cement). I: Transition from twinned crystals of calcite striations to calcite gouge, and to calcite coating with thin micritic interlayer (mi). J: Gradual decrease in CL colors through the striations-gouge-coating transition. Note the uniform bright CL color of completely recrystallized calcite striations. Location is shown in B.

1. Calcite cement precipitates (denoted "T") occur within dilation breccias and veins (Fig. 2A) and are characterized by equidimensional coarse-grained crystals (up to 5 mm in size) with sutured grain boundaries and thick straight twinning (Fig. 2C). Under CL light, the calcite cement shows bright CL colors and crystal zoning (Fig. 2D).

2. Calcite striation precipitates (denoted "S") occur in small dilation sites within the fault surface and are commonly associated with striated groove morphology (Figs. 2A and 2B). Calcite crystals are equidimensional coarse-grained and twinned. Sutured grain boundaries are marked with bright CL colors, in contrast to the dark CL colors of the host grains (Fig. 2F). Completely crystallized grains show no zoning and have uniform bright CL colors (Fig. 2J).

3. Calcite gouge precipitates (denoted "X") are fine-grained, reddish-colored calcite precipitates that appear opaque under polarized light (Fig. 2I). They are characterized by dark CL colors (Fig. 2J) and occur either within complex veinlet networks (e.g., within trans-granular fractures; Fig. 2H), surrounding breccia fragments (Fig. 2A), or coating fault surfaces (Fig. 2B).

4. Calcite coating precipitates (denoted "Y") occur as an ~1–3-mm-thick layer in the outermost part of the striated fault plane (Figs. 2G–2J). Grains are blocky to elongated-blocky (Figs. 2B and 2I), with no luminescence or zoning (Fig. 2J). In several samples, the coating layer consists of a parallel sequence of elongated-blocky twinned calcite crystals with growth-competition textures, interlayered with fine-grained micritic layers (Fig. 2I). SEM images of the uppermost part of the coating layer (Fig. 2G), parallel to the striation, show perfect rhombic crystal shapes with no indication of grain-size reduction.

Trace Elements, C-O-Sr Isotopes, and U-Th Dating

The stable isotope data, $^{87}Sr/^{86}Sr$ ratios, and chondrite-normalized rare earth element and yttrium (REY) patterns highlight two main groups (Fig. 3; Table DR1 in the Data Repository). The first group is characterized by values of $\delta^{18}O$ (~20‰), $\delta^{13}C$ (~ −5.5‰), and $^{87}Sr/^{86}Sr$ (~0.7075) that are either lower than or equal to those of the host-rock limestone, and high Sr and REY concentrations. In addition, REY patterns are similar to those

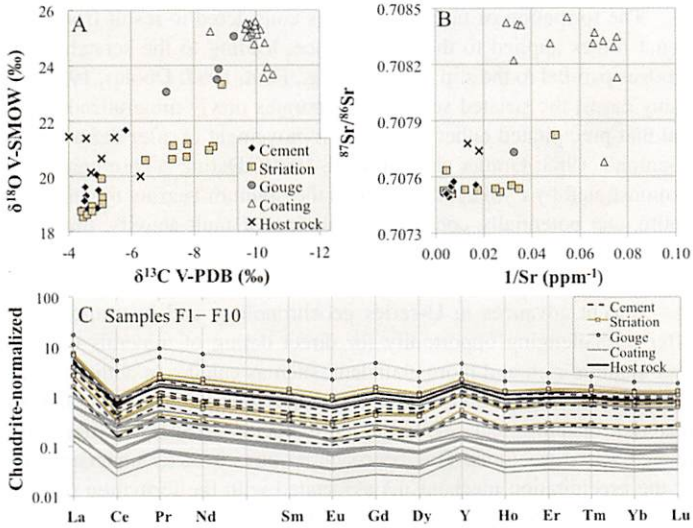

Figure 3. Geochemical results of fault-related calcite precipitates and host-rock samples. A: $\delta^{18}O$ (Vienna standard mean ocean water [V-SMOW]) versus $\delta^{13}C$ (Vienna Peedee belemnite [V-PDB]) in per mil (‰). B: $^{87}Sr/^{86}Sr$ versus reciprocal of Sr concentration (ppm^{-1}) plot. C: Chondrite-normalized rare earth element and yttrium patterns of the different types of calcite precipitates relative to their host rocks for samples F1, F6, F7, and F10. Calcite types are marked with different symbols. Chondrite values are from Haskin et al. (1971).

[1]GSA Data Repository item 2012168, Figures DR1–DR3 (sampling location and description) and Table DR1 (analytical procedures and results), is available online at www.geosociety.org/pubs/ft2012.htm, or on request from editing@geosociety.org or Documents Secretary, GSA, P.O. Box 9140, Boulder, CO 80301, USA.

of the host-rock limestone, with well-defined Ce-negative and Y-positive anomalies (Fig. 3C). In contrast, the second group is characterized by high $\delta^{18}O$ (~25‰), low $\delta^{13}C$ (~ −10‰), high $^{87}Sr/^{86}Sr$ (up to 0.7084), minor Ce-negative and Y-positive anomalies, and low Sr and REY concentrations (Figs. 3A–3C). Overall, the calcite cement and striations are more closely related to the first group, whereas the calcite coating layer is more closely related to the second group. The calcite gouge is scattered in between the two groups, and its REY concentrations are slightly higher than those of the host rock (Fig. 3C).

The U-Th age results indicate that calcite precipitation within the striated fault planes occurred between 220 ± 2.2 and 61 ± 0.5 ka (2σ). U-Th age determinations of the calcite gouge were mostly unsuccessful due to the presence of insoluble clay material, except for one sample that did not have indications for insoluble material (sample P23-GX1). A summary of the ages of the different types of calcite precipitates is presented in Figure 4 and in Table DR1.

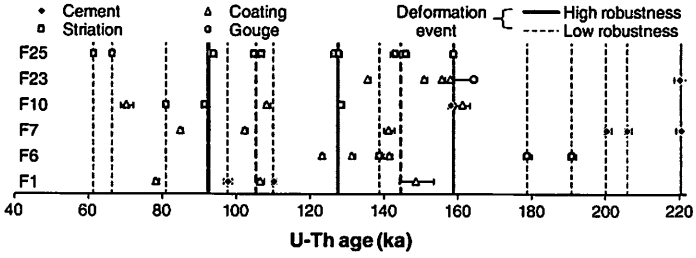

Figure 4. U-Th ages of calcite precipitates within striated fault planes. Sample names are denoted at the left side. U-Th ages have ±2σ error bars (symbols may be larger than error bars). Solid lines indicate well-defined (high-robustness) deformation events characterized by coeval development of syntectonic precipitates (calcite cement and striations). Samples from the calcite coating layer are suggested to form during interseismic periods (see text). Dashed lines indicate moderately defined (low-robustness) deformation events based on single-sample age constraints. The timing of the deformation events is based on the age error of the dated samples, with maximum of ±1 ka (represented by line thickness).

DISCUSSION

Mechanism of Calcite Precipitation Within Striated Fault Planes

Microstructural observations within the calcite cement and striations show equidimensional coarse-grained calcite and radial growth textures (Figs. 2B and 2C), which are indicative of fast calcite precipitation in dilation sites associated with seismic fault sliding (Gratier and Gamond, 1990). In contrast, evidence for crack-seal fibers, associated with slow dissolution and precipitation (Gratier and Gamond, 1990), was not observed. Additional CL observations show that calcite within sutured grain boundaries ("S2" in Fig. 2F), groove-related dilation sites ("S" in Fig. 2J), and dilation breccia ("T" in Fig. 2D) has distinct bright CL colors. This phase of precipitation could form by pressure solution and crystallization during deformation, which was enhanced within grain boundaries and asperities along the fault surface. Dated samples of calcite striations are characterized by homogeneous bright CL colors ("S" in Fig. 2J), indicating complete crystallization during a single precipitation event. Thus, we interpret the U-Th ages of calcite striations as the timing of deformation (Fig. 4). The observation of zoning in calcite cement (Figs. 2C and 2D) may suggest precipitation over a longer period, possibly during a cluster of seismic events.

Additional evidence for the process of pressure solution is found in the geochemistry of the calcite cement and striations. Their REY composition and chondrite-normalized REY patterns are similar to those of the host-rock limestone (Fig. 3), suggesting that these precipitates originated from pressure solution of the host rock with various contributions from local fluids, as described in other fluid systems within the Dead Sea fault zone (Janssen et al., 2005). This process possibly occurred by nonequilibrium fractionation during dissolution and/or precipitation, as indicated by the lower $^{87}Sr/^{86}Sr$, $\delta^{18}O$, and $\delta^{13}C$ values of the calcite precipitates relative to the host rock. Kinetic effects due to relatively fast dissolution and/or precipitation rates are known to produce calcite enriched in lighter isotopes (DePaolo, 2011).

Calcite gouge was found within trans-granular fractures, forming a complex veinlet network (Fig. 2H), and in between the striations and calcite coating layer (Fig. 2I). While the former occurrence can be associated with injection by high fluid pressure during hydraulic fracturing (e.g., Lin, 1996), the latter occurrence is most likely related to pressure solution processes during deformation, whereby the insoluble clay residues were concentrated along the dilation-asperity boundaries (similar to stylolitization). The isotopic signature of the calcite gouge suggests the involvement of meteoric water, with various contributions from host-rock dissolutions. However, contributions from other fluid sources cannot be ruled out. Unlike typical fault gouge, which is a mixture of detrital and authigenic clays (e.g., Lin, 1996), calcite gouge from this study is a mixture of detrital clays, carbonate derived from the fault zone, and newly formed authigenic calcite. The U-Th analyses of sample P23-GX1 yield an age of 164 ka, which should be considered as a maximum age of precipitation due to the possible contribution of carbonate from the limestone host rock. This age is consistent with the microstructural evidence (Fig. 2H), in which calcite gouge appears to postdate the formation of calcite cement, and predate the formation of the calcite coating layer (220 and 159 ka, respectively; Fig. 4).

The microstructural and geochemical signatures of the calcite coating layer are analogous to those found in calcite speleothems and dilation veins. Their isotopic and elemental compositions correlate with coeval speleothems from northern Israel (Bar-Matthews et al., 2003), and with calcite-filled dilation veins from the same site (Nuriel et al., 2012). The combination of nonluminescence colors (Fig. 2I), low REY contents, high $\delta^{18}O$, low $\delta^{13}C$, and high Sr ratios (Fig. 3) suggests the involvement of meteoric water with various degrees of fluid-soil interaction and precipitation under low-temperature conditions. While the uppermost morphology of calcite coating (78–70 ka) shows no evidence for postprecipitation deformation (Fig. 2G), lower levels closer to the host-rock interface (151–85 ka) have morphologies such as twinning calcite and sheared surfaces (Fig. 2I), indicating possible development by an aseismic slip-seal mechanism.

Dating Brittle Deformation

The formation mechanisms of the various types of calcite precipitates within striated fault planes are shown to be directly linked to brittle deformation processes (i.e., dilation, brecciation, hydraulic fracturing, and faulting). Therefore, the U-Th ages of these precipitates can be used to constrain the timing of deformation events, the robustness of which depends on the quality and quantity of the dated materials. We refer to a deformation age as being robust if it is supported by coeval U-Th ages of syntectonic precipitates (calcite cement and striations) from at least two localities. In contrast, low-robustness age constraints are based only on a single U-Th age of syntectonic precipitates. The calcite coating is interpreted to form during interseismic creep and/or fault relaxation-extension, and its age provides an additional constraint on the transition between interseismic and seismic fault activity. Following these criteria, four well-defined deformation events are identified, at 220, 159, 128, and 93 ka (solid lines in Fig. 4).

The dated events could be associated with periods of intense seismicity, and could potentially correlate with independent paleoseismic records from the Dead Sea fault zone. However, such records are limited for the period between 220 and 60 ka. One available paleoseismic record is from the central sector of the Dead Sea fault zone, ~170 km south of the study

area (Kagan et al., 2005). In this record, major paleoearthquakes were inferred from U-Th ages obtained in the immediate vicinity of damaged cave deposits. The well-defined deformation event at 128 ka correlates with the paleoearthquake event reported by Kagan et al. (2005). In addition, the moderately defined (low-robustness) deformation events at 178, 110, 105, and 98 ka also overlap with those proposed by Kagan et al. (2005). Further U-Th ages from striated fault planes, combined with independent paleoseismic records from the central sector of the Dead Sea fault zone, may shed light on the robustness of these deformation events.

CONCLUSIONS

The results of this study document a prolonged history (~160 k.y.) of calcite precipitation localized along striated fault planes. The results indicate that calcite precipitated in temporal association with brittle deformation processes such as dilation and faulting (calcite cement and striations), hydraulic fracturing (calcite gouge), and interseismic precipitation along fault planes (calcite coating). Four well-defined deformation events (i.e., seismically active periods) are constrained by coeval ages from different localities. One of these events (128 ka) correlates with an independent record of paleoearthquakes along the Dead Sea fault zone. This study demonstrates that faulting and striation in limestone involve calcite precipitation during the various stages of the seismic cycle. Therefore, this highlights the applicability of U-Th dating of calcite-filled microstructures within striated fault planes for constraining the timing of brittle deformation.

ACKNOWLEDGMENTS

The manuscript benefited from constructive comments by two anonymous reviewers and the editor Patience Cowie. We wish to thank Wan-Ping Hu, Kim Baublys, and Kim Sewell for assistance with ICP-MS analyses, stable isotope mass spectrometry, and scanning electron microscopy, respectively. We acknowledge the support of ARC grants LE0989067 and DP0773081.

REFERENCES CITED

Bar-Matthews, M., Ayalon, A., Gilmour, M., Matthews, A., and Hawkesworth, C.J., 2003, Sea-land oxygen isotopic relationships from planktonic foraminifera and speleothems in the Eastern Mediterranean region and their implication for paleorainfall during interglacial intervals: Geochimica et Cosmochimica Acta, v. 67, p. 3181–3199, doi:10.1016/S0016-7037(02)01031-1.

Boles, J.R., and Grivetti, M., 2000, Calcite cementation along the Refugio/Carneros fault, Coastal California: A link between deformation, fluid movement and fluid-rock interaction at a basin margin: Journal of Geochemical Exploration, v. 69–70, p. 313–316, doi:10.1016/S0375-6742(00)00065-0.

Boullier, A.-M., Fujimoto, K., Ohtani, T., Roman-Ross, G., Lewin, E., Ito, H., Pezard, P., and Ildefonse, B., 2004, Textural evidence for recent co-seismic circulation of fluids in the Nojima fault zone, Awaji Island, Japan: Tectonophysics, v. 378, p. 165–181, doi:10.1016/j.tecto.2003.09.006.

DePaolo, D.J., 2011, Surface kinetic model for isotopic and trace element fractionation during precipitation of calcite from aqueous solutions: Geochimica et Cosmochimica Acta, v. 75, p. 1039–1056, doi:10.1016/j.gca.2010.11.020.

Doblas, M., 1998, Slickenside kinematic indicators: Tectonophysics, v. 295, p. 187–197, doi:10.1016/S0040-1951(98)00120-6.

Eyal, Y., Kaufman, A., and Bar-Matthews, M., 1992, Use of $^{230}Th/U$ ages of striated carnotites for dating fault displacements: Geology, v. 20, p. 829–832, doi:10.1130/0091-7613(1992)020<0829:UOTUAO>2.3.CO;2.

Flotté, N., Plagnes, V., Sorel, D., and Benedicto, A., 2001, Attempt to date Pleistocene normal faults of the Corinth-Patras Rift (Greece) by U/Th method, and tectonic implications: Geophysical Research Letters, v. 28, p. 3769–3772, doi:10.1029/2001GL012964.

Gamond, J.F., 1983, Displacement features associated with fault zones: A comparison between observed examples and experimental models: Journal of Structural Geology, v. 5, p. 33–45, doi:10.1016/0191-8141(83)90005-6.

Garfunkel, Z., 1981, Internal structure of the Dead Sea leaky transform (rift) in relation to plate kinematics: Tectonophysics, v. 80, p. 81–108, doi:10.1016/0040-1951(81)90143-8.

Gratier, J.P., and Gamond, J.F., 1990, Transition between seismic and aseismic deformation in the upper crust, *in* Knipe, R.J., and Rutter, E.H., eds., Deformation mechanisms, rheology and tectonics: The Geological Society of London Special Publication 54, p. 461–473.

Haskin, L.A., Helmke, P.A., Paster, T.P., and Allen, R.O., 1971, Rare earths in meteoritic, terrestrial, and lunar matter, *in* Brunfelt, A., and Steinnes, E., eds., Activation analysis in geochemistry and cosmochemistry: Oslo, Universitetsforlaget, p. 201–218.

Janssen, C., Romer, R.L., Hoffmann-Rothe, A., Mingram, B., Dulski, P., Möller, P., and Al-Zubi, H., 2005, The role of fluids in faulting deformation: A case study from the Dead Sea Transform (Jordan): International Journal of Earth Sciences, v. 94, p. 243–255, doi:10.1007/s00531-004-0461-0.

Kagan, E.J., Agnon, A., Bar-Matthews, M., and Ayalon, A., 2005, Dating large infrequent earthquakes by damaged cave deposits: Geology, v. 33, p. 261–264, doi:10.1130/G21193.1.

Laurent, P., 1987, Shear-sense determination on striated faults from *e* twin lamellae in calcite: Journal of Structural Geology, v. 9, p. 591–595, doi:10.1016/0191-8141(87)90144-1.

Lin, A., 1996, Injection veins of crushing-originated pseudotachylyte and fault gouge formed during seismic faulting: Engineering Geology, v. 43, p. 213–224, doi:10.1016/0013-7952(96)00062-2.

Nuriel, P., Rosenbaum, G., Uysal, I.T., Zhao, J.-X., Golding, S.D., Weinberger, R., Karabacak, V., and Avni, Y., 2011, Formation of fault-related calcite precipitates and their implications for dating fault activity in the East Anatolian and Dead Sea fault zones, *in* Fagereng, Å., et al., eds., Geology of the earthquake source: A volume in honour of Rick Sibson: The Geological Society of London Special Publication 359, p. 229–248.

Nuriel, P., Weinberger, R., Rosenbaum, G., Golding, S.D., Zhao, J.-X., Uysal, I.T., Bar-Matthews, M., and Gross, M.R., 2012, Timing and mechanism of late-Pleistocene calcite vein formation across the Dead Sea Fault Zone, northern Israel: Journal of Structural Geology, v. 36, p. 43–54.

Petit, J.P., 1987, Criteria for the sense of movement on fault surfaces in brittle rocks: Journal of Structural Geology, v. 9, p. 597–608, doi:10.1016/0191-8141(87)90145-3.

Uysal, I.T., Feng, Y., Zhao, J.-X., Altunel, E., Weatherley, D., Karabacak, V., Cengiz, O., Golding, S.D., Lawrence, M.G., and Collerson, K.D., 2007, U-series dating and geochemical tracing of late Quaternary travertine in co-seismic fissures: Earth and Planetary Science Letters, v. 257, p. 450–462, doi:10.1016/j.epsl.2007.03.004.

Verhaert, G., Muchez, P., Sintubin, M., Similox-Tohon, D., Vandycke, S., and Waelkens, M., 2003, Reconstruction of neotectonic activity using carbonate precipitates: A case study from the northwestern extremity of the Isparta Angle (SW Turkey): Journal of Geochemical Exploration, v. 78–79, p. 197–201, doi:10.1016/S0375-6742(03)00070-0.

Verhaert, G., Muchez, P., Sintubin, M., Similox-Tohon, D., Vandycke, S., Keppens, E., Hodge, E.J., and Richards, D.A., 2004, Origin of palaeofluids in a normal fault setting in the Aegean region: Geofluids, v. 4, p. 300–314, doi:10.1111/j.1468-8123.2004.00094.x.

Watanabe, Y., Nakai, S.I., and Lin, A., 2008, Attempt to determine U-Th ages of calcite veins in the Nojima fault zone, Japan: Geochemical Journal, v. 42, p. 507–513, doi:10.2343/geochemj.42.507.

Weinberger, R., Gross, M.R., and Sneh, A., 2009, Evolving deformation along a transform plate boundary: Example from the Dead Sea Fault in northern Israel: Tectonics, v. 28, TC5005, doi:10.1029/2008TC002316.

Zhou, H.Y., Zhao, J., Wang, Q., Feng, Y.X., and Tang, J., 2011, Speleothem-derived Asian summer monsoon variations in Central China during 54–46 ka: Journal of Quaternary Science, v. 26, p. 781–790, doi:10.1002/jqs.1506.

Manuscript received 27 October 2011
Revised manuscript received 30 January 2012
Manuscript accepted 13 February 2012

Printed in USA